ISSN 0006-2979, Biochemistry (Moscow), 2024, Vol. 89, No. 2, pp. 257-268 © Pleiades Publishing, Ltd., 2024.

Safari with an Electron Gun: Visualization of Protein and Membrane Interactions in Mitochondria in Natural Environment

Semen V. Nesterov[1,a]*, Konstantin S. Plokhikh[1], Yuriy M. Chesnokov[1], Denis A. Mustafin[1], Tatyana N. Goleva[1], Anton G. Rogov[1], Raif G. Vasilov[1], and Lev S. Yaguzhinsky[2]

[1]*National Research Center "Kurchatov Institute," 123182 Moscow, Russia*

[2]*Belozersky Research Institute for Physico-Chemical Biology, Lomonosov Moscow State University, 119992 Moscow, Russia*

[a]*e-mail: semen.v.nesterov@phystech.edu*

Received September 24, 2023
Revised February 6, 2024
Accepted February 7, 2024

Abstract—This paper presents new structural data about mitochondria using correlative light and electron microscopy (CLEM) and cryo-electron tomography. These state-of-the-art structural biology methods allow studying biological objects at nanometer scales under natural conditions. Non-invasiveness of these methods makes them comparable to observing animals in their natural environment on a safari. The paper highlights two areas of research that can only be accomplished using these methods. The study visualized location of the Aβ42 amyloid aggregates in relation to mitochondria to test a hypothesis of development of mitochondrial dysfunction in Alzheimer's disease. The results showed that the Aβ42 aggregates do not interact with mitochondria, although some of them are closely located. Therefore, the study demonstrated that mitochondrial dysfunction is not directly associated with the effects of aggregates on mitochondrial structure. Other processes should be considered as sources of mitochondrial dysfunction. Second unique area presented in this work is high-resolution visualization of the mitochondrial membranes and proteins in them. Analysis of the cryo-ET data reveals toroidal holes in the lamellar structures of cardiac mitochondrial cristae, where ATP synthases are located. The study proposes a new mechanism for sorting and clustering protein complexes in the membrane based on topology. According to this suggestion, position of the OXPHOS system proteins in the membrane is determined by its curvature. High-resolution tomography expands and complements existing ideas about the structural and functional organization of mitochondria. This makes it possible to study the previously inaccessible structural interactions of proteins with each other and with membranes *in vivo*.

DOI: 10.1134/S0006297924020068

Keywords: membrane, mitochondria, oxidative phosphorylation, cryo-electron microscopy, supercomplex, ATP synthase, respirasome, Aβ42, amyloid aggregates

INTRODUCTION

In recent years, cryogenic-electron microscopy (cryo-EM) techniques have undergone significant improvements in both hardware and software. These improvements have led to a breakthrough in structural biology with increased availability and comprehensive image processing capabilities [1-3]. While many

Abbreviations: ATP, adenosine triphosphate; CLEM, correlative light and electron microscopy; cryo-EM, cryogenic electron microscopy; cryo-ET, cryogenic electron tomography; OXPHOS, oxidative phosphorylation; TEM, transmission electron microscopy.

* To whom correspondence should be addressed.

microscopy studies are investigating isolated proteins with high resolution, we will narrow our focus on macromolecular organization of the enzyme systems in mitochondrial membranes in whole mitochondria without isolating proteins from them. This article demonstrates capabilities of the correlative light and electron microscopy (CLEM) [4]. CLEM, in combination with genetic engineering, allows visualization of interactions between any proteins of interest, as well as between proteins and membranes, with a resolution of a few nanometers. CLEM outperforms solely light-based techniques in terms of resolution, including super-resolution microscopy such as STED microscopy [5]. STED microscopy allows visualization of membranes but not individual proteins within them [6]. In this work, we present our new results, deeply analyze a number of tomographic data obtained in our previous works, and discuss the literature devoted to "photoelectron hunting" of mitochondrial proteins in 'wild' natural conditions of their existence in protein–lipid membranes.

Despite the considerable amount of structural data on mitochondrial proteins, the data on their native positions in the membrane and matrix are very limited, which makes it difficult to form an integral model of the work of these organelles. Recently, cryo-EM has helped to fill this gap in our understanding. For example, it has been found that adenosine triphosphate (ATP) synthases in the mammalian mitochondria are located at the folds of the inner membrane (cristae), while components of the respiratory chain are located in the less curved parts of the membrane. Additionally, much information has emerged on the structural interaction of respiratory chain complexes (respirasome). However, many questions still remain unanswered. Standard laboratory methods for extracting respirasomes with a mild detergent cannot provide reliable information on the percentage of respiratory chain complexes that form respirasomes. This is because some complexes disintegrate during the extraction process, and some could be not extracted from the membrane. Simultaneously, a detailed analysis of cryo-EM tomograms enables us to solve this problem. For instance, we demonstrated that all complexes I and III are part of respirasomes in the rat heart [7]. Data from numerous scientific groups indicate that proton transfer between the proton pumps and ATP synthase occurs not due to electrochemical gradient between the matrix and intermembrane space volumes, but rather occurs locally with protons moving laterally along the membrane surface for short distances. A detailed study of the structure of mitochondrial membranes and proteins can provide unique information necessary for testing existing hypotheses and modeling proton transfer processes in the oxidative phosphorylation system (OXPHOS) [8]. Additionally, many structural aspects of interaction between mitochondria and other organelles or various aggregates are still unknown. Even interaction of amyloid aggregates with mitochondrial membrane remains poorly investigated despite high prevalence of Alzheimer's disease. However, colocalization of the fluorescent tags does not provide sufficient resolution for unambiguous conclusions. In this study, we were able to answer this question using correlative light-electron microscopy.

MATERIALS AND METHODS

Cultivation of yeast cells. *Yarrowia lipolytica* Po1f yeast expressing eGFP-Aβ42 construct [9] were used in this work. Cells were grown in 250-ml Erlenmeyer flasks at 28°C on a rotary shaker (220 rpm) in 50 ml of semi-synthetic medium containing 1.3% succinate as a carbon and energy source. Cells were harvested in the early exponential growth phase (OD_{600} = 1.0).

Preparation of samples for cryo-EM. Cells were rinsed with 50 mM phosphate buffer (pH = 5.5) to remove the growth medium. Next, they were incubated with 500 nM MitoTracker Red CMXRos for 30 min. Afterward, the cells were washed to remove the dye and concentrated to OD_{600} = 25. To minimize formation of ice crystals, 5% glycerol was added to the suspension before plating it on a cryo-EM grid [10]. Electron microscopy grids underwent hydrophilization using a Pelco easiGlow unit (USA) at 25 mA current and 0.26 mBar pressure for 30 s. Next, a 5-μl aliquot of cell suspension was applied to a microscopy grid. Extra liquid from the grids with the test objects was removed from both sides using filter paper and next grids were subjected to quick freezing in a liquefied ethane cooled to liquid nitrogen temperature. When applying the sample to the grid, temperature in the chamber of the Thermo Fisher Scientific Vitrobot system (USA) was maintained at 4°C, and humidity was at least 95%. If homogenate of cardiac tissue or isolated rat heart mitochondria were used, a similar grid preparation procedure was performed, but without the use of glycerol, as described in the previously published works [7, 11]. Briefly, 3 μl of homogenized Wistar rat heart tissue or isolated cardiac mitochondria (isolated using differential centrifugation, without the use of detergents or proteases, as previously described [12]) were applied to a microscopy grid and vitrified using a Vitrobot system.

Fluorescence microscopy. Vitrified yeast samples were placed in a cryogenic chamber of a Leica THUNDER Imager EM Cryo CLEM fluorescence microscope (Germany) equipped with a Leica HC PL APO 50×/0.90 CRYO CLEM objective (Germany). Fluorescence of eGFP-Aβ42 and MitoTracker Red was recorded using appropriate filters, and colocalization of eGFP-Aβ42 and mitochondrial aggregates were assessed. The Leica Thunder

algorithm was used to perform 3D reconstruction of yeast cells, followed by image deconvolution with the aid of embedded software [13]. Images of the entire grid provided a "map" for orientation during lamella etching. Regions of interest were selected based on the images obtained from the entire grid.

Preparation of lamellae by focused ion beam (FIB). The vitrified sample on microscopic grids was transferred to a Thermo Fisher Scientific Versa 3D scanning electron ion microscope (USA) equipped with a cryoprobe and a Quorum 3100P liquid nitrogen temperature sample loading system. To reduce charge accumulation and protect surface from radiation damage during the experiment, a gas-injection system was used to sputter a protective layer of platinum on the entire grid surface. Based on the surface morphology and fluorescence microscopy maps, we selected areas for preparing thin cell slices using cryo-FIB (Fig. 1). We have chosen regions closer to the center of the grid where the cells were arranged in a single layer. The lamellae were cut in these squares with expectation of passing along a few cells located at a sufficient distance from the metal framework of the grid. Gallium ions with an energy of 30 keV were used to minimize radiation damage to the near-surface layer. The current was sequentially reduced from 1 nA to 30 pA. This approach produced object slices with 150-250 nm thickness. The slice plane was inclined at an angle of 10-12° with respect to the plane of the microscopic grid.

Cryo-EM and cryo-ET. Cryo-EM studies were performed using a Thermo Fisher Scientific Titan Krios 60-300 cryogenic transmission electron microscope (USA) at accelerating voltage of 300 kV, equipped with a Falcon II direct electron detection system. For each microscopic grid, sections were selected to obtain rotating series of images. Each dataset consisted of 56 images taken by tilting the sample between –50° and 60° in 2° angular increments. Data acquisition was performed automatically using a Thermo Fisher Scientific Tomography 4 software (USA) in low dose mode, which minimized radiation damage while preserving native structure of the studied objects. Magnification of 18,000× (pixel size 0.37 nm and image size 1516 nm) with a defocus value in the range [–5 μm; –8 μm] was used to set the tomographic series. Total electron dose passing through a unit area of the sample during the entire exposure time did not exceed ~120 $e^{-}/Å^{2}$.

Data processing. Tomographic reconstruction procedure using the Weighted Back Projections (WBP) method in the IMOD software package [14] was applied to the obtained data. Alignment of the rotated series of cell images was performed by calculating cross-correlation between the regions of the tomographic series (the "patch tracking" procedure [15]), since it is impossible to introduce colloidal gold nanoparticles into the sample. In the case of studying fragments of the isolated mitochondria, colloidal gold nanoparticles with 10 nm diameter were used to achieve higher resolution [7, 16].

In order to reduce noise and resolution anisotropy in different planes of the obtained tomograms, filtering in the IsoNet program was used [17]. This tool uses a U-net neural network and is trained on small sections of tomograms with addition of extra noise. Segmentation of mitochondrial membranes was performed in an automatic mode using the program TomoSegMemTV [18]. Errors in the automatic segmentation were corrected manually using the original tomogram data.

The tomograms after filtering were used in manual mode to determine positions of different molecular complexes. Positions and orientations of various macromolecules were also determined automatically using three-dimensional templates of these molecules in the Dynamo [19] or WARP [20] programs. Subsequent iterative 3D classification was performed to eliminate incorrectly selected coordinates. To increase the signal-to-noise ratio and spatial resolution [21] of macromolecules, averaging of small sections of the tomogram (called subtomograms) containing individual macromolecules aligned with each other was used [22]. This process, called subtomographic averaging, simultaneously provides information about orientation of macromolecules, which is used for subsequent visualization of the object by inserting a model of the averaged structure in the desired orientation.

RESULTS

Visualization of amyloid aggregates in cells. Based on fluorescence microscopy data, it has previously been suggested that the beta-amyloid (Aβ42) aggregates can interact with mitochondrial membranes and thereby disrupt bioenergetics [9]. For the experiment, we have chosen a previously used model based on the aerobically metabolizing yeast *Y. lipolytica* expressing the eGFP-Aβ42 construct [9]. It was shown earlier that expression of Aβ42 or of eGFP-Aβ42 reporter gene construct led to dysfunction and fragmentation of yeast mitochondria [9]. Colocalization of amyloid aggregates and mitochondria revealed in this work [9] led to the hypothesis of direct physical contact of amyloid aggregates with the mitochondrial membrane. To test this hypothesis, a CLEM microscopy protocol was performed, culminating in cryo-electron tomography (cryo-ET) of the selected regions of interest. It is important to note that cryo-ET is the only suitable method of investigation for this task, because during the vitrification process and subsequent microscopic examination, native structure of the samples is practically not disturbed, which is an important parameter

because fluorescent objects are located at a small distance and even a slight change in their colocalization due to the use of standard technique of fixing and contrasting the sample for electron microscopy could lead to the appearance of artifacts.

The cryogenic CLEM protocol involved using fluorescence microscopy to examine the vitrified sample for the most representative fields of view where MitoTracker Red-stained mitochondria and fluorescent eGFP-Aβ42 aggregates were expected to colocalize. Once a region of interest was identified, z-stack imaging was performed to reconstruct 3D location of the areas containing mitochondria and eGFP-Aβ42 aggregates. Based on this information, FIB was adjusted to obtain a lamella containing the region of interest for which cryo-electron tomograms were obtained. Figure 1 shows the intermediate results of each stage of the study.

As a result, a series of detailed tomograms of the regions of interest were obtained, superimposing both mitochondrial fluorescence (red channel, MitoTracker Red) and amyloid aggregates (green channel, eGFP-Aβ42). At the same time, resolution of the cryo-electron tomograms was significantly higher than that of the fluorescence microscope, allowing us to distinguish both membranes and individual proteins in the mitochondria that have characteristic structural features, such as ATP synthases (Fig. 1d). The eGFP fluorescence signal allowed to localize amyloid aggregates, which could not be clearly identified without fluorescent labeling and using CLEM. The aggregates were shown not to interact with the mitochondrial membrane. As can be seen in Fig. 1, some of the aggregates do not localize near the mitochondria at all, which can also be seen in the fluorescence microscopy images. As for the ambiguous areas where the fluorescence signals overlap, statistical data were collected for several dozen of aggregates in these areas (Fig. 2) and it was shown that the vast majority of aggregates were

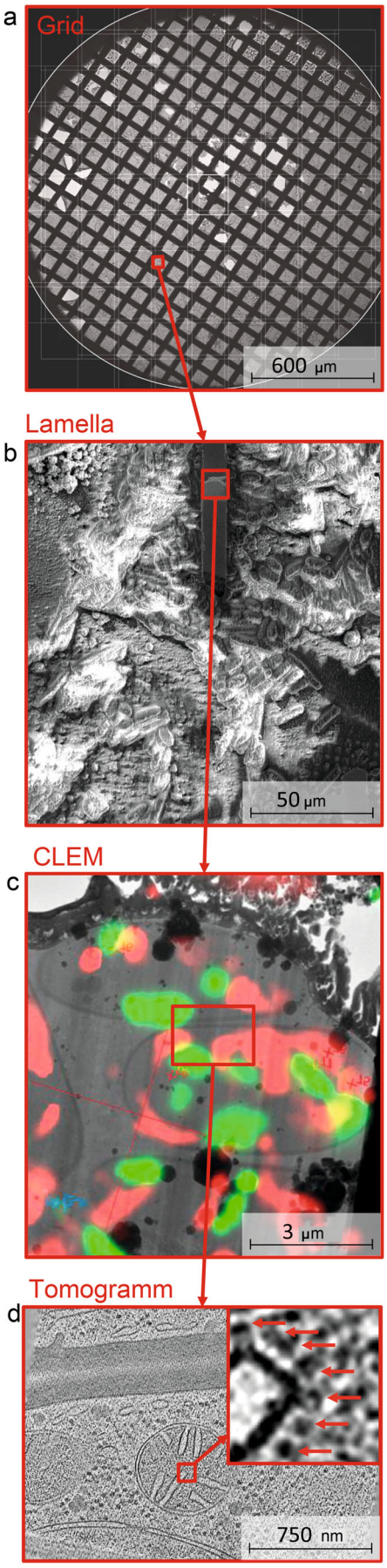

Fig. 1. Workflow on a cell sample during CLEM microscopy combined with cryo-ET. a) Photograph of a grid with a vitrified sample under a transmission light microscope. b) Magnified image of the area highlighted in panel (a) with sputtered platinum layer and an area cut out by cryogenic focused ion beam method in which there is a thin lamella (highlighted with a red frame). Scanning electron ion microscopy image. c) Correlative light and electron microscopy (CLEM) of the lamella. Overlay of the fluorescence image region corresponding to the etched lamella. Red fluorescence is MitoTracker Red (mitochondrial marker), green fluorescence is eGFP (from the eGFP-Aβ42 construct). d) Slice of the tomogram plotted against the region inside the lamella showing two mitochondria as well as other cell components (cell wall, ribosomes, amyloid aggregates and various vesicular structures). Inset shows an enlarged fragment of a mitochondrial crista, with red arrows pointing at F1 subunits of ATP synthase protruding from the membrane.

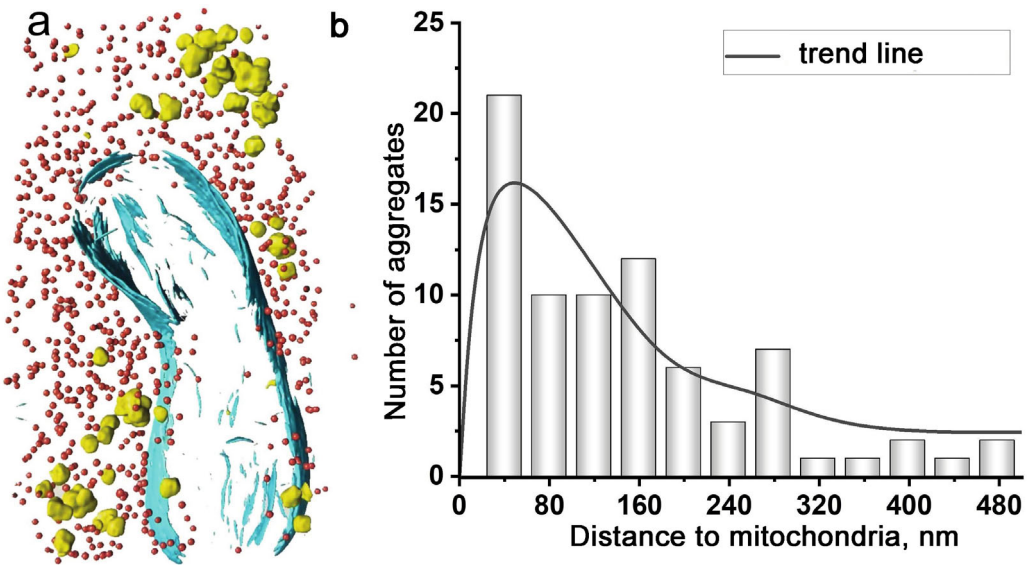

Fig. 2. Visualization and estimation of distances between Aβ42 aggregates and mitochondrial outer membrane on multiple tomograms. a) Example of computer reconstruction of a tomogram with automatically labeled mitochondrial membranes (blue), amyloid aggregates (yellow) and ribosomes (red). b) Distribution of distances between the aggregates and the mitochondrial outer membrane assembled from the tomographic data.

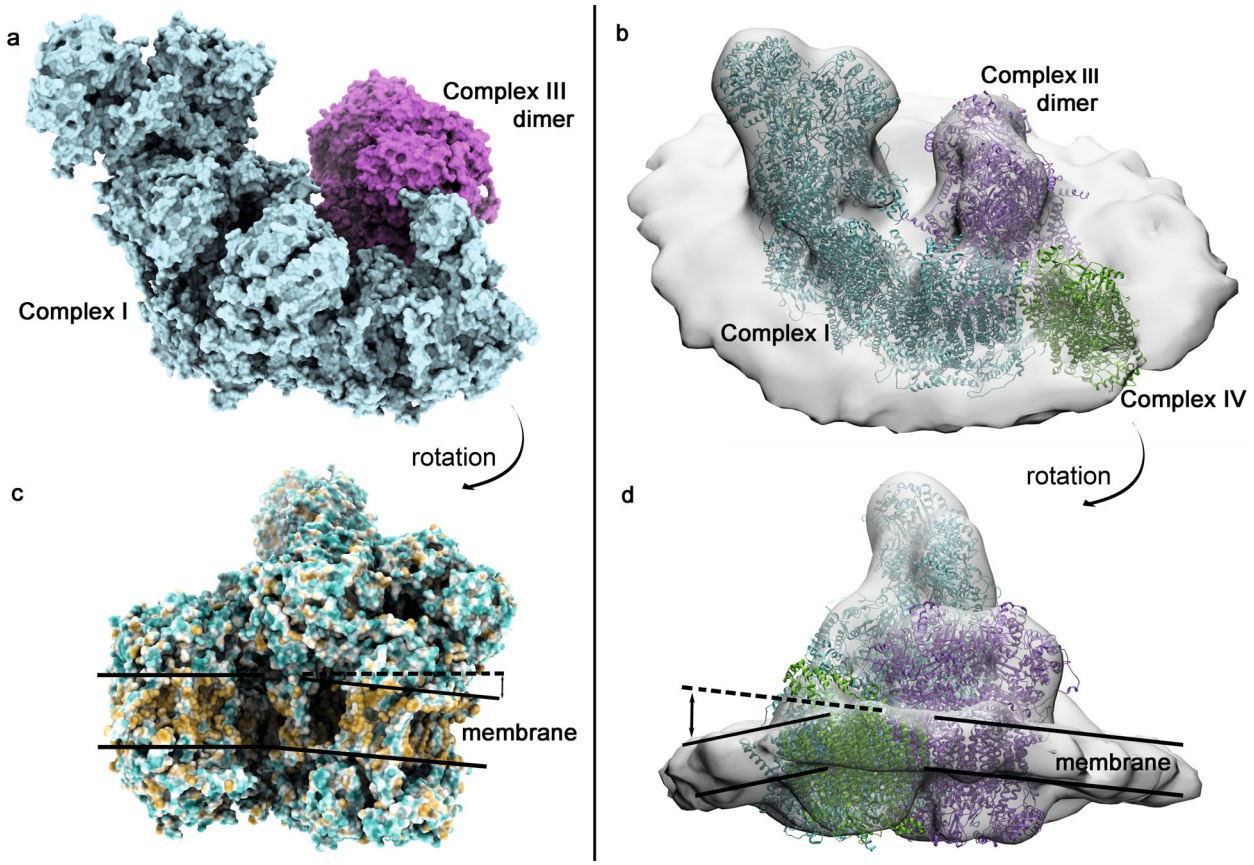

Fig. 3. Structures of the respiratory chain supercomplex of mitochondria from different organisms. a, c) Different projections of the respirasome surface structure from *Arabidopsis* sp. mitochondria obtained by single-particle cryo-EM (resolution about 2 Å, PDB ID: 8BPX) [34]. b, d) Different projections of the respirasome structure from rat heart mitochondria obtained by subtomographic averaging without extraction of the respirasome from the membrane according to [7]. In panels (a), (b), (c) different complexes within the supercomplex [blue – complex I, purple – complex III, green – complex IV (only present in rat respirasomes)] are highlighted by different colors. In panel (c) color mapping is done according to the surface hydrophilicity (blue – hydrophilic, yellow – hydrophobic) to better illustrate presence of the membrane curvature.

located at a distance of 30-300 nm from the mitochondrial membrane surface.

The closest aggregates had no physical contacts with the mitochondrial membrane. This finding is important for understanding the mechanisms of Alzheimer's disease development, as it suggests that the disturbance in mitochondrial bioenergetics that correlates with aggregate accumulation [23, 24] is not caused by the direct effect of amyloid aggregates on mitochondrial structure and function, but is mediated by other factors.

Study of the topology of the inner mitochondrial membrane and proteins of the OXPHOS system within it. The single-particle cryo-EM method, based on computer classification and averaging of huge arrays of images obtained by transmission electron microscopy (TEM), allows us to study structures of large protein complexes and supercomplexes. Presence or absence of supercomplexes has long been a controversial topic in bioenergetics, yet this fact is extremely important. Presence of supercomplexes implies direct transfer of metabolites between them with minimal involvement of diffusion in this process. Such arrangement is much more resistant to stress, reduces electron leakage and ROS generation, making the whole system more energy efficient. Existence of large respiratory chain supercomplexes in mitochondria prior to the use of cryo-EM was demonstrated by the presence of common migration of their components during native electrophoresis after protein extraction from membranes with mild detergents [25]. Nowadays, existence of the respiratory supercomplexes – respirasomes – is no longer in doubt due to cryo-EM imaging of single particles, as their structures from different organisms and tissues have been demonstrated in a large number of studies [26-33]. Nevertheless, more detailed issues, such as exact configuration and composition of supercomplexes under certain conditions, their functional, regulatory and structural significance for bioenergetics, remain controversial. In particular, mechanisms of regulation by respirasomes, existence of any structural interaction between them and ATP synthases, and role of the membrane in these processes are not fully understood. To address these issues, we analyzed the data obtained in our previous studies together with the new literature data. Figure 3 shows structures of the respirasomes from the evolutionarily distant *Arabidopsis* sp. mitochondria and rat heart mitochondria, which surprisingly turned out to be not only similar in structure, but also to have a similar curvature of the membrane, creating its kink at the point of contact of complexes I and III.

Cryo-ET (cryo-electron tomography) allows us to reconstruct entire membrane regions by determining location of the proteins with characteristic structural features. Such proteins include ATP synthases and complexes I, which have unique shape of a large hydrophilic part protruding from the membrane (Fig. 4, a, b). In addition, it is possible to reconstruct three-dimensional structure of the inner mitochondrial membrane with resolution that significantly exceeds that of tomography, based on analysis of the slices of fixed mitochondrial samples. As a result, cryo-ET shows the inner membranes of cardiac mitochondria in greater detail and are not represented as wave-like lamellar structures, as interpreted from the TEM ultrathin sections [35], but as a complex structure of many small flat fragments interspersed with many tubular junctions (Fig. 4). This structure answers the question of how ATP synthase dimers are arranged in the inner membrane of cardiac mitochondria. The most abundant oligomers of ATP synthases are found at the bends of the highly curved cristae [36], but there are fewer long clusters of ATP synthases in the regions with lower curvature, where a less ordered structure is created in which dense packing of respirasomes and ATP synthases is impossible (Fig. 4b, right row of ATP synthases).

On a smaller scale (without visualization of individual membrane proteins), it is possible to perform a detailed reconstruction of the inner membrane of cardiac mitochondria using high resolution images generated with cryo-ET. We have recently performed such reconstruction to visualize position of the large dehydrogenase complexes relative to the membrane under natural conditions [11]. The obtained data suggest (Fig. 4) that the cardiac mitochondria are a complex maze of highly curved membranes with a lamellar-tubular structure. At the same time, ATP synthase dimers cannot be located in the completely lamellar flat areas [36]. From the point of view of ensuring optimal structure and functionality of mitochondria, the lamellar structure of the membrane seems to be unsuitable for accommodating the key components of OXPHOS. This issue can be partially resolved by formation of the wave-like curved structures of the inner membrane bilayer, on the curved areas of which ATP synthases can be localized. Such topology has been indeed observed in some TEM images [37]. However, the membrane structures are often visualized as lamellar, which prevents formation even of the strained structures with ATP synthase dimers, one of which is shown in Fig. 4b. The paradox of the presence of lamellae visible by classical electron microscopy was resolved by using higher resolution of cryo-ET. The computer reconstruction showed that toroidal holes are formed in the lamellar regions at the edges of which ATP synthase dimers could be located, and close to them in the regions with less curvature – respirasomes. In contrast to the cristae edges shown in Fig. 3, the toroidal openings at the edges could accommodate not only one row of ATP synthase dimers, but even two rows of the tightly at-

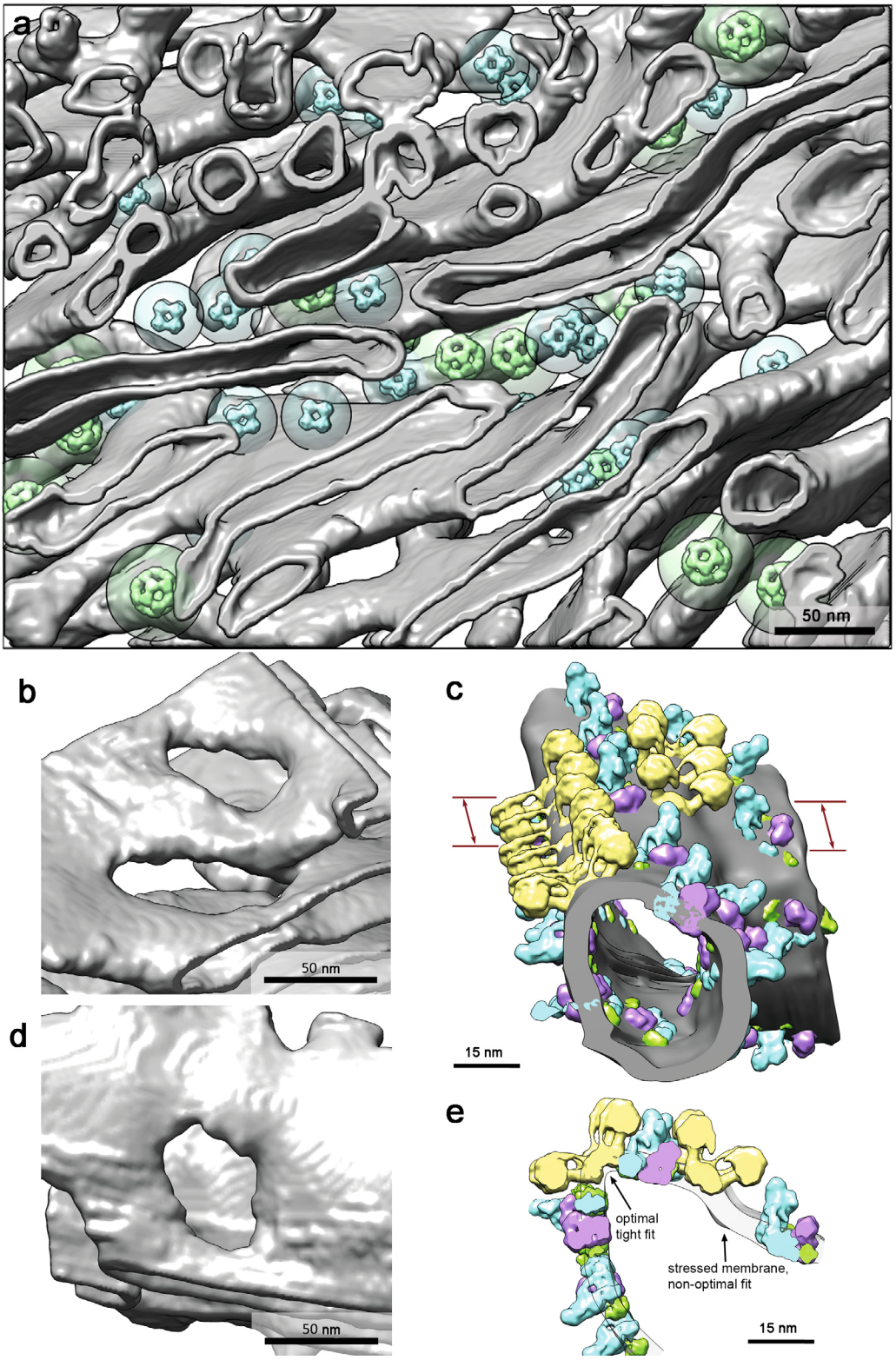

Fig. 4. Reconstruction of the complex structure of the mitochondrial membranes of the heart. a) Reconstruction of a tomogram of a large area in a whole intact mitochondrion of the rat heart. Blue – cores of ketoglutarate dehydrogenase or branched-chain ketoacid dehydrogenase complexes, green – cores of pyruvate dehydrogenase complexes. b, d) Fragments illustrating presence of holes of toroidal topology. c) Reconstruction of a fragment of a tomogram of a rat heart mitochondrial crista. ATP synthases are shown in yellow, complexes I in blue, dimers of complexes III in purple and complexes IV in green. The membrane shown in grey is not transparent and covers hydrophobic parts of the complexes. e) Thin section of part of the crista at the location indicated by the arrows in panel (c). The membrane is shown transparent, allowing visualization of the hydrophobic parts of the complexes. The image created based on the tomographic data obtained in the course of previous work [7, 11].

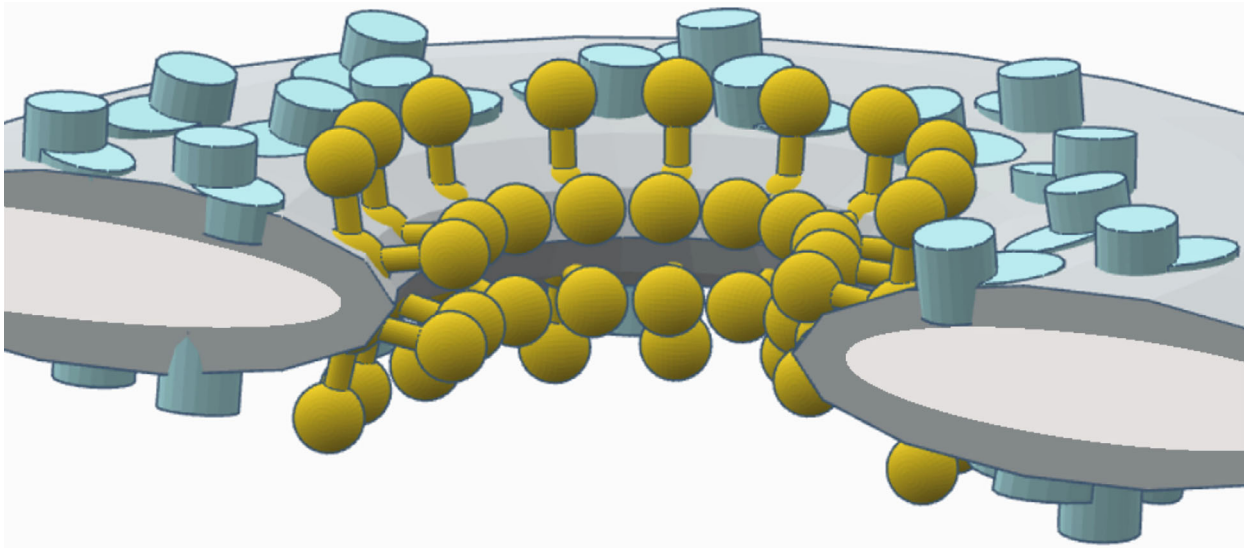

Fig. 5. Schematic model of putative location of protein complexes of the OXPHOS system in the vicinity of toroidal holes in the pseudolamellar regions of cristae. The model was constructed based on manual processing of cryo-ET images of several toroidal holes with labelling of the location of F1 subunits of ATP synthases in the inner membrane of rat heart mitochondria. Yellow indicates ATP synthase dimers, blue indicates respirasomes, dark grey indicates membrane and light grey indicates intermembrane space.

tached ATP synthases. This ensures the most efficient use of the rather small (compared to the total area of the cristae) curved regions of the membrane for locating ATP synthase dimers on them. An oligomeric structure of the ATP synthase dimers similar to that shown in Fig. 4 has been observed in the toroidal holes in the region with high curvature. However, the preliminary manual analysis shows a larger number of structures in some of the toroidal holes that correspond in size to the F1 subunits of ATP synthases, suggesting that the two rows of ATP synthase dimers may be present at the membrane fold at the same time. Due to the high protein density, which prevents high resolution, accurate computer reconstruction using averaging of ATP synthases in these regions has not yet been possible. Schematic representation of the proposed arrangement of the OXPHOS complexes in such structures is shown in Fig. 5.

This complex topology of mitochondrial membranes may be maintained by high concentration of the cone-shaped lipids such as cardiolipin and phosphatidylethanolamine in the membrane. Presumably, the membrane junctions are so enriched in these lipids, and their structure is so different from the bilayer, that they have been defined by NMR as a non-bilayer lipid phase [37, 38]. Given the necessity of cardiolipin for operation of the OXPHOS system [39] and optimization of its structure to ensure proton transport across the membrane [8], we can assume that the propensity of respirasomes and ATP synthases to generate membrane curvature may, at least in part, be evolutionarily determined by the need for cardiolipin concentration at the interface of OXPHOS system proteins.

DISCUSSION

Lack of direct interaction of amyloid aggregates with mitochondrial membranes. Advanced models of chronic diseases associated with mitochondrial dysfunction, based on the aerobic metabolic yeast *Y. lipolytica* [9], have proven to be a powerful tool to reveal intracellular actions of the markers of these diseases, which is an important task in the case of pathologies associated with mitochondrial dysfunction [40], since mitochondria are quite deeply involved in the cell signaling systems, and it is often difficult to understand whether their dysfunction is primary or mediated by pathological changes in the cellular environment. The yeast *Y. lipolytica*, as a unicellular organism, lacks complex system of intercellular interactions and, in addition, possesses a branched system of fully functional “animal-type” mitochondria containing all the complexes of the respiratory chain.

It was shown [9] that the Aβ42 expression in the yeast caused mitochondrial dysfunction, which is characteristic for the neurons at the early stages of Alzheimer’s disease development. In addition, colocalization of mitochondria and amyloid aggregates suggested the presence of physical contact between the mitochondria and amyloid aggregates, as assumed in some other work [41]. Since vitrification of the samples for cryogenic microscopy is the least destructive method of object fixation, the data obtained in this work could be considered as the most reliable showing absence of the contact between the amyloid protein aggregates and mitochondria.

Nevertheless, distribution of the distances between the aggregates and mitochondrial membrane indicates

concentration of aggregates near mitochondria, which may be essential for the processes of mitochondrial substrate transport or for the effects of aggregates on the protein biosynthesis due to the large number of ribosomes also located near mitochondria.

Model of topological coupling of supercomplexes in the mitochondrial membrane. An interesting peculiarity that was identified owing to cryo-ET was the fact that the ATP synthases not only dimerize (this can be detected by native electrophoresis), but also form oligomeric arrays that deform the membrane and induce a significant curvature on it [16, 42, 43]. It turns out that respirasomes also affect membrane curvature, as shown in the cryo-EM images of respirasomes from different organisms [30, 34]. Furthermore, interaction of the complex I and complex III dimers in respirasome is conserved, and structure of the respirasome is highly similar between the species [44] suggesting that interaction of the respirasome with the membrane is also conserved. This implies that association of respirasomes with ATP synthases shown in [7] (Fig. 4c) could be achieved largely through the mechanical properties of the membrane, which tend to compensate for excessive tension. The ATP synthase dimers create a region of maximum membrane curvature close to them [36], thereby creating tension in the bilayer and distorting it from the energetically optimal structure that would be present if the lipids self-assembled in the absence of the protein. In the region away from ATP synthases, the membrane tends to approach the equilibrium topology of a lamellar bilayer. At the same time, respirasomes also generate membrane tension, but the lipid bilayer around them has much less curvature than near the ATP synthase dimers. In order for respirasomes not to create a separate region of membrane curvature, it is advantageous for them to be located closer to ATP synthases in the part of the membrane where the curvature is already optimal for them and no additional energy is required to mechanically distort the lipid bilayer. In such case, preferential orientation of respirasomes along one axis should be observed, which is indeed confirmed by the experiments with cardiac mitochondria [7]. Thus, the force attracting respirasomes to ATP synthase has an entropic topological nature and is determined by the membrane, which tends to minimize its deviation from the approximate equilibrium bilayer structure. It should also be noted that the integral protein complexes that create curvature of the mitochondrial membrane also create around themselves membrane domains (rafts) of cardiolipin and other lipids that have conical shape, since they are the ones best suited to create curvature in the lipid bilayer [45]. Binding of ATP synthases and respiratory complexes (both individually and assembled into respirasomes) to cardiolipin has been repeatedly confirmed in experiments [38, 46-53]. Ability of cardiolipin to form membrane domains has also been experimentally demonstrated [54].

Sorting of the proteins based on their interaction with membrane lipids is well known – such sorting system based on rafts and nanorafts operates in the cell [55]. Sorting of the proteins in membrane rafts is mainly based on coincidence or mismatch of the thickness of their hydrophobic membrane zone with the thickness of a certain cluster of membrane lipids (hydrophobic mismatch principle). The above data on mitochondrial membranes allow us to add to the well-known principle of clustering of proteins with similar hydrophobic zone another sorting principle based on affinity of the protein complexes to the zones of different membrane curvature. Complex topology of the inner membrane of cardiac mitochondria and presence of the non-bilayer phases in it suggest that self-organization of the OXPHOS system complexes in the cardiac mitochondria could proceed via the mechanism similar to the *in meso* crystallization of membrane proteins [56].

Thus, the above data suggest that the structure of respirasomes is evolutionarily selected to ensure localization of respirasomes close to ATP synthase dimers and thus clustering of the entire OXPHOS system through interaction with the membrane lipids.

CONCLUSION

This work demonstrates experimental application of one of the most advanced methods in structural biology to study interaction of protein aggregates with membranes, topology of the membranes themselves, and mutual arrangement of membrane proteins in mitochondria under native conditions. A series of new experiments using CLEM have shown that amyloid aggregates do not interact with the outer mitochondrial membrane and do not enter the mitochondria. In addition, our own recent data and recent literature data obtained using cryogenic-electron transmission microscopy and tomography of mitochondria and mitochondrial membranes have been analyzed in more detail. Complex arrangement and intricate topology of the rat heart mitochondrial membranes, enriched in large supercomplexes that influence membrane curvature, are shown. In complete agreement with this, it was shown that the cardiac mitochondrial membrane has only small regions where it is close to a flat bilayer, whereas most of the membrane is a complex network of highly curved junctions on which rows of ATP synthase dimers and respiratory chain supercomplexes are located. The regions of the membrane that appear lamellar on the TEM thin sections are actually dotted with a multitude of holes containing tightly packed clusters of protein complexes of the OXPHOS system.

This paper also discusses theoretical framework that explains clustering of the membrane proteins of the OXPHOS system and cardiolipin by minimization of the strain energy of the lipid part of the membrane. This principle of membrane protein organisation is proposed to be termed topological.

Contributions. S.V.N. planned and performed experiments, manually analyzed tomograms, prepared the manuscript; D.A.M., T.N.G., and A.G.R. planned and conducted CLEM experiments with yeast; K.S.P. and Yu.M.Ch. conduct TEM and CLEM experiments, perform computer processing of the tomographic data. L.S.Y. and R.G.V. developed the study concept, supervised the study. All authors discussed the results and contribute to the manuscript editing.

Funding. This work was financially supported by the NRC Kurchatov Institute (thematic plan 1f.4.1 "Study of energy generation, transfer and distribution processes in living organisms aimed at finding new approaches to the development of therapeutic agents, new bioenergetic devices and artificial photosynthesis systems").

Ethics declarations. This work does not contain any studies involving human and animal subjects. The authors of this work declare that they have no conflicts of interest.

REFERENCES

1. Saibil, H. R. (2022) Cryo-EM in molecular and cellular biology, *Mol. Cell*, **82**, 274-284, doi: 10.1016/j.molcel.2021.12.016.
2. Guaita, M., Watters, S. C., and Loerch, S. (2022) Recent advances and current trends in cryo-electron microscopy, *Curr. Opin. Struct. Biol.*, **77**, 102484, doi: 10.1016/j.sbi.2022.102484.
3. Chua, E. Y. D., Mendez, J. H., Rapp, M., Ilca, S. L., Tan, Y. Z., Maruthi, K., Kuang, H., Zimanyi, C. M., Cheng, A., Eng, E. T., Noble, A. J., Potter, C. S., and Carragher, B. (2022) Better, faster, cheaper: recent advances in cryo-electron microscopy, *Annu. Rev. Biochem.*, **91**, 1-32, doi: 10.1146/annurev-biochem-032620-110705.
4. Hoffman, D. P., Shtengel, G., Xu, C. S., Campbell, K. R., Freeman, M., Wang, L., Milkie, D. E., Pasolli, H. A., Iyer, N., Bogovic, J. A., Stabley, D. R., Shirinifard, A., Pang, S., Peale, D., Schaefer, K., Pomp, W., Chang, C.-L., Lippincott-Schwartz, J., Kirchhausen, T., Solecki, D. J., Betzig, E., and Hess, H. F. (2020) Correlative three-dimensional super-resolution and block-face electron microscopy of whole vitreously frozen cells, *Science*, **367**, eaaz5357, doi: 10.1126/science.aaz5357.
5. Liu, T., Stephan, T., Chen, P., Keller-Findeisen, J., Chen, J., Riedel, D., Yang, Z., Jakobs, S., and Chen, Z. (2022) Multi-color live-cell STED nanoscopy of mitochondria with a gentle inner membrane stain, *Proc. Natl. Acad. Sci. USA*, **119**, e2215799119, doi: 10.1073/pnas.2215799119.
6. Wang, C., Taki, M., Sato, Y., Tamura, Y., Yaginuma, H., Okada, Y., and Yamaguchi, S. (2019) A photostable fluorescent marker for the superresolution live imaging of the dynamic structure of the mitochondrial cristae, *Proc. Natl. Acad. Sci. USA*, **116**, 15817-15822, doi: 10.1073/pnas.1905924116.
7. Nesterov, S., Chesnokov, Y., Kamyshinsky, R., Panteleeva, A., Lyamzaev, K., Vasilov, R., and Yaguzhinsky, L. (2021) Ordered clusters of the complete oxidative phosphorylation system in cardiac mitochondria, *Int. J. Mol. Sci.*, **22**, 1462, doi: 10.3390/ijms22031462.
8. Nesterov, S. V., Yaguzhinsky, L. S., Vasilov, R. G., Kadantsev, V. N., and Goltsov, A. N. (2022) Contribution of the collective excitations to the coupled proton and energy transport along mitochondrial cristae membrane in oxidative phosphorylation system, *Entropy*, **24**, 1813, doi: 10.3390/e24121813.
9. Epremyan, K. K., Rogov, A. G., Goleva, T. N., Lavrushkina, S. V., Zinovkin, R. A., and Zvyagilskaya, R. A. (2023) Altered mitochondrial morphology and bioenergetics in a new yeast model expressing Aβ42, *Int. J. Mol. Sci.*, **24**, 900, doi: 10.3390/ijms24020900.
10. Bischof, J., Hunt, C. J., Rubinsky, B., Burgess, A., and Pegg, D. E. (1990) Effects of cooling rate and glycerol concentration on the structure of the frozen kidney: Assessment by cryo-scanning electron microscopy, *Cryobiology*, **27**, 301-310, doi: 10.1016/0011-2240(90)90029-4.
11. Plokhikh, K. S., Nesterov, S. V., Chesnokov, Y. M., Rogov, A. G., Kamyshinsky, R. A., Vasiliev, A. L., Yaguzhinsky, L. S., and Vasilov, R. G. (2023) Association of 2-oxoacid dehydrogenase complexes with respirasomes in mitochondria, *FEBS J.*, **291**, 16965, doi: 10.1111/febs.16965.
12. Nesterov, S. V., Skorobogatova, Y. A., Panteleeva, A. A., Pavlik, L. L., Mikheeva, I. B., Yaguzhinsky, L. S., and Nartsissov, Y. R. (2018) NMDA and GABA receptor presence in rat heart mitochondria, *Chem. Biol. Interact.*, **291**, 40-46, doi: 10.1016/j.cbi.2018.06.004.
13. Sibarita, J.-B. (2005) Deconvolution microscopy, in *Microscopy Techniques* (Rietdorf, J., ed) Springer, Berlin, Heidelberg, pp. 201-243, doi: 10.1007/b102215.
14. Kremer, J. R., Mastronarde, D. N., and McIntosh, J. R. (1996) Computer visualization of three-dimensional image data using IMOD, *J. Struct. Biol.*, **116**, 71-76, doi: 10.1006/jsbi.1996.0013.
15. Wan, W., and Briggs, J. A. G. (2016) *Cryo-Electron Tomography and Subtomogram Averaging*, 1st Edn., Elsevier, doi: 10.1016/bs.mie.2016.04.014.
16. Nesterov, S. V., Chesnokov, Yu. M., Kamyshinsky, R. A., Yaguzhinsky, L. S., and Vasilov, R. G. (2020) Determining the structure and location of the ATP synthase in the membranes of rat's heart mitochondria using

cryoelectron tomography, *Nanotechnol. Russia*, **15**, 83-89, doi: 10.1134/S1995078020010139.

17. Liu, Y.-T., Zhang, H., Wang, H., Tao, C.-L., Bi, G.-Q., and Zhou, Z. H. (2022) Isotropic reconstruction for electron tomography with deep learning, *Nat. Commun.*, **13**, 6482, doi: 10.1038/s41467-022-33957-8.
18. Martinez-Sanchez, A., Garcia, I., Asano, S., Lucic, V., and Fernandez, J. J. (2014) Robust membrane detection based on tensor voting for electron tomography, *J. Struct. Biol.*, **186**, 49-61, doi: 10.1016/j.jsb.2014.02.015.
19. Castaño-Díez, D., Kudryashev, M., Arheit, M., and Stahlberg, H. (2012) Dynamo: A flexible, user-friendly development tool for subtomogram averaging of cryo-EM data in high-performance computing environments, *J. Struct. Biol.*, **178**, 139-151, doi: 10.1016/j.jsb.2011.12.017.
20. Tegunov, D., and Cramer, P. (2019) Real-time cryo-electron microscopy data preprocessing with Warp, *Nat. Methods*, **16**, 1146-1152, doi: 10.1038/s41592-019-0580-y.
21. Bharat, T. A. M., and Scheres, S. H. W. (2016) Resolving macromolecular structures from electron cryo-Tomography data using subtomogram averaging in RELION, *Nat. Protoc.*, **11**, 2054-2065, doi: 10.1038/nprot.2016.124.
22. Asano, S., Fukuda, Y., Beck, F., Aufderheide, A., Förster, F., Danev, R., and Baumeister, W. (2015) A molecular census of 26S proteasomes in intact neurons, *Science*, **347**, 439-442, doi: 10.1126/science.1261197.
23. Ashleigh, T., Swerdlow, R. H., and Beal, M. F. (2023) The role of mitochondrial dysfunction in Alzheimer's disease pathogenesis, *Alzheimers Dement. J. Alzheimers Assoc.*, **19**, 333-342, doi: 10.1002/alz.12683.
24. Bhatia, S., Rawal, R., Sharma, P., Singh, T., Singh, M., and Singh, V. (2022) Mitochondrial dysfunction in Alzheimer's disease: opportunities for drug development, *Curr. Neuropharmacol.*, **20**, 675-692, doi: 10.2174/1570159X19666210517114016.
25. Eubel, H., Heinemeyer, J., and Braun, H.-P. (2004) Identification and characterization of respirasomes in potato mitochondria, *Plant Physiol.*, **134**, 1450-1459, doi: 10.1104/pp.103.038018.
26. Chaban, Y., Boekema, E. J., and Dudkina, N. V. (2014) Structures of mitochondrial oxidative phosphorylation supercomplexes and mechanisms for their stabilization, *Biochim. Biophys. Acta*, **1837**, 418-426, doi: 10.1016/j.bbabio.2013.10.004.
27. Dudkina, N. V., Kouřil, R., Peters, K., Braun, H.-P., and Boekema, E. J. (2010) Structure and function of mitochondrial supercomplexes, *Biochim. Biophys. Acta*, **1797**, 664-670, doi: 10.1016/j.bbabio.2009.12.013.
28. Bultema, J. B., Braun, H.-P., Boekema, E. J., and Kouril, R. (2009) Megacomplex organization of the oxidative phosphorylation system by structural analysis of respiratory supercomplexes from potato, *Biochim. Biophys. Acta*, **1787**, 60-67, doi: 10.1016/j.bbabio.2008.10.010.
29. Dudkina, N. V., Kudryashev, M., Stahlberg, H., and Boekema, E. J. (2011) Interaction of complexes I, III, and IV within the bovine respirasome by single particle cryoelectron tomography, *Proc. Natl. Acad. Sci. USA*, **108**, 15196-15200, doi: 10.1073/pnas.1107819108.
30. Mühleip, A., Flygaard, R. K., Baradaran, R., Haapanen, O., Gruhl, T., Tobiasson, V., Maréchal, A., Sharma, V., and Amunts, A. (2023) Structural basis of mitochondrial membrane bending by the I-II-III2-IV2 supercomplex, *Nature*, **615**, 934-938, doi: 10.1038/s41586-023-05817-y.
31. Guo, R., Zong, S., Wu, M., Gu, J., and Yang, M. (2017) Architecture of human mitochondrial respiratory megacomplex I2III2IV2, *Cell*, **170**, 1247-1257.e12, doi: 10.1016/j.cell.2017.07.050.
32. Gu, J., Wu, M., Guo, R., Yan, K., Lei, J., Gao, N., and Yang, M. (2016) The architecture of the mammalian respirasome, *Nature*, **537**, 639-643, doi: 10.1038/nature19359.
33. Vercellino, I., and Sazanov, L. A. (2021) Structure and assembly of the mammalian mitochondrial supercomplex CIII2CIV, *Nature*, **598**, 364-367, doi: 10.1038/s41586-021-03927-z.
34. Klusch, N., Dreimann, M., Senkler, J., Rugen, N., Kühlbrandt, W., and Braun, H.-P. (2023) Cryo-EM structure of the respiratory I + III2 supercomplex from *Arabidopsis thaliana* at 2 Å resolution, *Nat Plants.*, **9**, 142-156, doi: 10.1038/s41477-022-01308-6.
35. Kühlbrandt, W. (2015) Structure and function of mitochondrial membrane protein complexes, *BMC Biol.*, **13**, 89, doi: 10.1186/s12915-015-0201-x.
36. Strauss, M., Hofhaus, G., Schröder, R. R., and Kühlbrandt, W. (2008) Dimer ribbons of ATP synthase shape the inner mitochondrial membrane, *EMBO J.*, **27**, 1154-1160, doi: 10.1038/emboj.2008.35.
37. Garab, G., Yaguzhinsky, L. S., Dlouhý, O., Nesterov, S. V., Špunda, V., and Gasanoff, E. S. (2022) Structural and functional roles of non-bilayer lipid phases of chloroplast thylakoid membranes and mitochondrial inner membranes, *Prog. Lipid. Res.*, **86**, 101163, doi: 10.1016/j.plipres.2022.101163.
38. Gasanov, S. E., Kim, A. A., Yaguzhinsky, L. S., and Dagda, R. K. (2018) Non-bilayer structures in mitochondrial membranes regulate ATP synthase activity, *Biochim. Biophys. Acta*, **1860**, 586-599, doi: 10.1016/j.bbamem.2017.11.014.
39. Paradies, G., Paradies, V., De Benedictis, V., Ruggiero, F. M., and Petrosillo, G. (2014) Functional role of cardiolipin in mitochondrial bioenergetics, *Biochim. Biophys. Acta*, **1837**, 408-417, doi: 10.1016/j.bbabio.2013.10.006.
40. Epremyan, K. K., Goleva, T. N., Rogov, A. G., Lavrushkina, S. V., Zinovkin, R. A., and Zvyagilskaya, R. A. (2022) The first *Yarrowia lipolytica* yeast models expressing

hepatitis B virus X protein: changes in mitochondrial morphology and functions, *Microorganism*, **10**, 1817, doi: 10.3390/microorganisms10091817.
41. Völgyi, K., Badics, K., Sialana, F. J., Gulyássy, P., Udvari, E. B., Kis, V., Drahos, L., Lubec, G., Kékesi, K. A., and Juhász, G. (2018) Early presymptomatic changes in the proteome of mitochondria-associated membrane in the APP/PS1 mouse model of Alzheimer's disease, *Mol. Neurobiol.*, **55**, 7839-7857, doi: 10.1007/s12035-018-0955-6.
42. Buzhynskyy, N., Sens, P., Prima, V., Sturgis, J. N., and Scheuring, S. (2007) Rows of ATP synthase dimers in native mitochondrial inner membranes, *Biophys. J.*, **93**, 2870-2876, doi: 10.1529/biophysj.107.109728.
43. Blum, T. B., Hahn, A., Meier, T., Davies, K. M., and Kühlbrandt, W. (2019) Dimers of mitochondrial ATP synthase induce membrane curvature and self-assemble into rows, *Proc. Natl. Acad. Sci. USA*, **116**, 4250-4255, doi: 10.1073/pnas.1816556116.
44. Davies, K. M., Blum, T. B., and Kühlbrandt, W. (2018) Conserved *in situ* arrangement of complex I and III2 in mitochondrial respiratory chain supercomplexes of mammals, yeast, and plants, *Proc. Natl. Acad. Sci. USA*, **115**, 3024-3029, doi: 10.1073/pnas.1720702115.
45. Beltrán-Heredia, E., Tsai, F.-C., Salinas-Almaguer, S., Cao, F. J., Bassereau, P., and Monroy, F. (2019) Membrane curvature induces cardiolipin sorting, *Commun. Biol.*, **2**, 225, doi: 10.1038/s42003-019-0471-x.
46. Arias-Cartin, R., Grimaldi, S., Arnoux, P., Guigliarelli, B., and Magalon, A. (2012) Cardiolipin binding in bacterial respiratory complexes: structural and functional implications, *Biochim. Biophys. Acta*, **1817**, 1937-1949, doi: 10.1016/j.bbabio.2012.04.005.
47. Arnarez, C., Marrink, S. J., and Periole, X. (2013) Identification of cardiolipin binding sites on cytochrome *c* oxidase at the entrance of proton channels, *Sci. Rep.*, **3**, 1263, doi: 10.1038/srep01263.
48. Duncan, A. L., Robinson, A. J., and Walker, J. E. (2016) Cardiolipin binds selectively but transiently to conserved lysine residues in the rotor of metazoan ATP synthases, *Proc. Natl. Acad. Sci. USA*, **113**, 8687-8692, doi: 10.1073/pnas.1608396113.
49. Pfeiffer, K., Gohil, V., Stuart, R. A., Hunte, C., Brandt, U., Greenberg, M. L., and Schägger, H. (2003) Cardiolipin stabilizes respiratory chain supercomplexes, *J. Biol. Chem.*, **278**, 52873-52880, doi: 10.1074/jbc.M308366200.
50. Mühleip, A., McComas, S. E., and Amunts, A. (2019) Structure of a mitochondrial ATP synthase with bound native cardiolipin, *eLife*, **8**, e51179, doi: 10.7554/eLife.51179.
51. Mileykovskaya, E., and Dowhan, W. (2014) Cardiolipin-dependent formation of mitochondrial respiratory supercomplexes, *Chem. Phys. Lipids*, **179**, 42-48, doi: 10.1016/j.chemphyslip.2013.10.012.
52. Zhang, M., Mileykovskaya, E., and Dowhan, W. (2005) Cardiolipin is essential for organization of complexes III and IV into a supercomplex in intact yeast mitochondria, *J. Biol. Chem.*, **280**, 29403-29408, doi: 10.1074/jbc.M504955200.
53. Zhang, M., Mileykovskaya, E., and Dowhan, W. (2002) Gluing the Respiratory Chain Together cardiolipin is required for supercomplex formation in the inner mitochondrial membrane, *J. Biol. Chem.*, **277**, 43553-43556, doi: 10.1074/jbc.C200551200.
54. Mileykovskaya, E., and Dowhan, W. (2009) Cardiolipin membrane domains in prokaryotes and eukaryotes, *Biochim. Biophys. Acta*, **1788**, 2084-2091, doi: 10.1016/j.bbamem.2009.04.003.
55. Diaz-Rohrer, B., Levental, K. R., and Levental, I. (2014) Rafting through traffic: Membrane domains in cellular logistics, *Biochim. Biophys. Acta*, **1838**, 3003-3013, doi: 10.1016/j.bbamem.2014.07.029.
56. Zabara, A., Meikle, T. G., Newman, J., Peat, T. S., Conn, C. E., and Drummond, C. J. (2017) The nanoscience behind the art of *in meso* crystallization of membrane proteins, *Nanoscale*, **9**, 754-763, doi: 10.1039/C6NR07634C.